The BErkeley Atmospheric CO_2 Observation Network: Field Calibration and Evaluation of Low-cost Air Quality Sensors

Jinsol Kim[1], Alexis A. Shusterman[2], Kaitlyn J. Lieschke[2], Catherine Newman[2], and Ronald C. Cohen[1,2]

[1]Department of Earth and Planetary Science, University of California Berkeley, Berkeley, CA 94720, USA
5   [2]Department of Chemistry, University of California Berkeley, Berkeley, CA 94720, USA

Correspondence to: Ronald C. Cohen (rccohen@berkeley.edu)

Abstract. The newest generation of air quality sensors is small, low cost, and easy to deploy. These sensors are an attractive option for developing dense observation networks in support of regulatory activities and scientific research. They are also of interest for use by individuals to characterize their home environment and for citizen science. However, these sensors are

10   difficult to interpret. Although some have an approximately linear response to the target analyte, that response may vary with time, temperature, and/or humidity, and the cross-sensitivity to non-target analytes can be large enough to be confounding. Standard approaches to calibration that are sufficient to account for these variations require a quantity of equipment and labor that negates the attractiveness of the sensors' low cost. Here we describe a novel calibration strategy for a set of sensors including CO, NO, NO_2, and O_3 that makes use of multiple co-located sensors, a priori knowledge about the

15   chemistry of NO, NO_2, and O_3, as well as an estimate of mean emission factors for CO and the global background of CO. The strategy requires one or more well calibrated anchor points within the network domain, but it does not require direct calibration of any of the individual low-cost sensors. The procedure nonetheless accounts for temperature and drift, in both the sensitivity and zero offset. We demonstrate this calibration on a subset of the sensors comprising $BEACO_2N$, a distributed network of approximately 50 sensor "nodes," each measuring CO_2, CO, NO, NO_2, O_3 and particulate matter at 10

20   second time resolution and approximately 2km spacing within the San Francisco Bay Area.

1 Introduction

In urban environments, air quality has complex spatial and temporal patterns. Diverse emission sources are present with large variations in emission rate and source type on scales of hundreds of meters. In addition, dispersion of pollutants into the urban environment is affected by the topography of the urban landscape and the associated wind flows, which also vary

25   on length scales of ~100 m (Vardoulakis et al., 2003; Lateb et al., 2016). Conventional approaches to air quality monitoring rely on a limited number of relatively high cost instruments that lack the spatial resolution needed to characterize these variations, opting instead to target spatial averages. This averaging hampers our attempts at source attribution and understanding of mixing, chemistry, and human exposure in cities where emissions vary on spatial scales that are small compared to typical observations or models.

1

One approach to obtaining higher spatial resolution observations is passive sampling, which has been implemented using inexpensive sampling devices that can be later analyzed in bulk. Passive samplers do not require electrical power to function properly and are collected and analyzed one to two weeks after deployment. Such protocols provide high spatial resolution but also have significant drawbacks. Spatial resolution is gained at the expense of temporal resolution, and analysis after collection of the samplers is time consuming, thus passive sampling has typically been used only in short duration experiments (e.g. Krupa & Legge, 2000; Cox, 2003). Furthermore, as a result of boundary layer dynamics, passive sampling in urban areas is likely dominated by the high concentrations found at night and relatively insensitive to daytime variability.

Recent developments in low-cost sensors for trace gases and particulate matter, as well as advances in software and hardware enabling low-cost data communication, have made high-density, high time resolution air quality monitoring networks possible. Devices and networks of devices are emerging that are low cost, report at a time resolution of seconds, and are capable of long-term deployment, providing potential for improvement over the two major weaknesses of passive sampling. Examples include metal oxide sensors used to measure O_3, CO, NO_2, and total VOCs (e.g. Williams et al., 2013; Bart et al., 2014; Piedrahita et al., 2014; Moltchanov et al., 2015; Sadighi et al., 2017), and electrochemical sensors used to measure CO, NO, NO_2, O_3, and SO_2 (e.g. Mead et al., 2013; Sun et al., 2015; Jiao et al., 2016; Hagan et al., 2017; Jerrett et al., 2017; Michael et al., 2017). These different low-cost sensor systems have been evaluated and compared (Borrego et al., 2016; Papapostolou et al., 2017). While these studies found low-cost trace gas sensors to be successful at qualitatively characterizing the variability of air quality in an urban area, challenges related to selectivity and stability remain, hindering more quantitative interpretation of the data.

The current generation of low-cost sensors is not as easily tied to a gravimetric calibration standard as many of the passive samplers. Calibration is known to vary with sensor age, temperature, and in some cases humidity. In addition, many of the sensors have responses to gases other than the target analyte (Mead et al., 2013; Spinelle et al., 2015; Cross et al., 2017; Michael et al., 2017; Mijling et al., 2017; Spinelle et al., 2017; Zimmerman et al., 2017). One approach to addressing this challenge is to combine periodic re-calibration and co-location with regulatory reference instruments in the lab or the field (Williams et al., 2013; Moltchanov et al., 2015; Jiao et al., 2016; Mijling et al., 2017). Field calibration is preferred as in-lab performance is often a poor approximation of sensor behavior under ambient conditions (Piedrahita et al., 2014; Masson et al., 2015). However, either method requires considerable time investment by trained personnel, especially as the number of sensors increases. The requirement of time- and labor-consuming calibration then offsets the low-cost advantage of the sensors.

In this paper, we explore an automated, in situ strategy for the calibration of individual sensors embedded in an air quality sensor network that includes both low-cost sensors and anchor points of higher grade, well calibrated instrumentation. The

BErkeley Atmospheric CO_2 Observation Network (BEACO$_2$N) is a low-cost, high-density greenhouse gas (CO_2) and air quality (CO, NO, NO_2, O_3, and particulate matter) monitoring network located in San Francisco Bay Area, California (see Fig. 1 and Shusterman et al., 2016). As of this writing, BEACO$_2$N consists of approximately 50 sensor "nodes," deployed with approximately 2 km horizontal spacing. Most of the nodes are mounted on the roofs of schools and museums. In previous work, we described an approach to CO_2 sensing and calibration (Shusterman et al. 2016). Here, we focus on CO, NO, NO_2, and O_3.

We begin by describing laboratory experiments and in-field comparisons to co-located reference instruments that give an initial characterization of the sensors and provide insight into the effects of temperature, humidity, and cross-sensitivity to non-target analytes. Then we describe an in situ calibration procedure that accounts for these variables without requiring co-location with a reference instrument. The calibration procedure is finally verified against regulatory quality measurements not used in the procedure itself.

2 Instrument Description

Details of the node design and deployment are described in Shusterman et al. (2016). Briefly, each BEACO$_2$N node contains a Vaisala CarboCap GMP343 non-dispersive infrared sensor for CO_2, a Shinyei PPD42NS nephelometric particulate matter sensor, and a suite of Alphasense electrochemical sensors: CO-B4, NO-B4, either NO_2-B42F or NO_2-B43F, and either O_x-B421 or O_x-B431. All sensors are assembled into compact, weatherproof enclosures as shown in Fig. 2. Two 30 mm fans are located on either side of the enclosure to facilitate airflow through the node. A Raspberry Pi microprocessor collects data via a serial-to-USB converter for CO_2 and an Adafruit Metro Mini microcontroller for all other sensors. Then, data collected every 5 or 10 seconds is transmitted to a central server using a direct on-site Ethernet connection or a local Wi-Fi network.

The Alphasense B4 electrochemical gas sensing series that we use employs a four-electrode approach. The electrodes are embedded in an electrolyte solution separated from the atmosphere by a semi-permeable membrane. The gas of interest diffuses through the membrane into the electrolyte where it contacts a "working" electrode, and is either oxidized (in the case of NO and CO) or reduced (NO_2 and O_3). The potential at the working electrode is maintained at a constant value with respect to a "reference" electrode. Electric charge produced at the working electrode is balanced by the complementary redox reaction at a "counter" electrode, generating an electric current. The sensor also contains an "auxiliary" electrode, which shares the working electrode's catalyst structure, but is isolated from the ambient environment, accounting for fluctuations in the background current associated with other processes at the electrode and electrolyte. Subtracting the auxiliary current from the working current gives a corrected current dependent on the gas concentration.

3

The working and auxiliary currents detected by the sensors are converted to working and auxiliary voltages using amplifiers in the Individual Sensor Boards (ISBs) provided by Alphasense. Over the mixing ratio range of interest, the sensors' responses to the gases of interest are approximately linear. We derive mixing ratios from the observed voltages by subtracting an offset and then scaling by a constant (Eqn. 1-4):

$$CO_{ambient} = (V_{CO} - zero_{CO})/k_{CO} \tag{1}$$

$$NO_{ambient} = (V_{NO} - zero_{NO})/k_{NO} \tag{2}$$

$$NO_{2ambient} = (V_{NO_2} - zero_{NO_2})/k_{NO_2} - (r_{NO-NO_2} \times NO_{ambient}) \tag{3a}$$

$$NO_{2ambient} = (V_{NO_2} - zero_{NO_2})/k_{NO_2} + (r_{NO-CO_2} \times CO_{2ambient}) \tag{3b}$$

$$O_{3ambient} = (V_{O_3} - zero_{O_3})/k_{O_3} - (r_{NO_2-O_3} \times NO2_{ambient}) \tag{4}$$

Here, CO, NO, NO$_2$, and O$_3$ with the subscript "ambient" refer to the gas mixing ratios (ppb) in air; V_{CO}, V_{NO}, V_{NO_2} and V_{O_3} are the signals (mV) measured by each sensor, which is the voltage of the auxiliary electrode subtracted from the voltage of the working electrode; $zero_{CO}$, $zero_{NO}$, $zero_{NO2}$ and $zero_{O3}$ indicates the voltage measured in the absence of analyte; and k_{CO}, k_{NO}, k_{NO_2} and k_{O_3} represent the linear sensitivity factor that converts mV to ppb. Additional terms corresponding to the cross-sensitivities of the NO$_2$ and O$_3$ sensors appear in Eqn. 3a, 3b, and 4, where r_{NO-NO_2} is the cross-sensitivity of the NO$_2$-B42F sensor to NO gas, r_{NO-CO_2} is the cross-sensitivity of the NO$_2$-B43F sensor to CO$_2$ gas, and $r_{NO_2-O_3}$ is the cross-sensitivity of both the O$_3$-B421 and O$_3$-B431 sensors to NO$_2$ gas.

There are a total of 8 sensitivities and zero offsets, as well as 2 cross-sensitivity terms. All of these may also vary with time, temperature, and humidity. Thus we need a calibration strategy that constrains 10 parameters in a single instant as well as the variation of those 10 parameters in response to the environmental variables and time. We begin by characterizing the sensors in both laboratory and outdoor environments.

We evaluate BEACO$_2$N in terms of four factors: drift, noise, cross-sensitivity, and temperature dependence. The humidity dependence is included in the temperature dependence, as there is no evidence for independent humidity dependence and relative humidity exhibits an anti-correlation with temperature in the field. In the laboratory, a range of mixing ratios of target gases were delivered to a chamber containing the full suite of four Alphasense B4 sensors: CO, NO, NO$_2$, and O$_3$. Zero air was supplied by a Sabio 1001 Compressed Zero Air Source and blended with calibration gases using a ThermoScientific 146i Multi-Gas Calibrator.

Noise – Alphasense reports 2σ noise of ±4 ppb, ±15 ppb, ±12 ppb, and ±15 ppb for CO, NO, NO$_2$, and O$_3$, respectively over concentrations from 0 ppb to 200 ppb at time resolution of a second. In our laboratory, noise (±2σ) was measured for

4

ambient ppb levels with 10-second time resolution and was seen to be ±10 ppb for CO, ±3 ppb for NO, ±6 ppb for NO_2 (NO_2-B42F and NO_2-B43F), and ±12 ppb for O_3 (O_3-B421 and O_3-B431).

Cross-Sensitivity – We measured the cross-sensitivity of all 4 of the trace gas sensors to the non-target gases. The NO_2
5   sensors and O_3 sensors were the only ones to exhibit sensitivity to other species. The O_3 sensor (O_3-B421 and O_3-B431) demonstrated 100% sensitivity to NO_2. This sensor is now being marketed by Alphasense as an odd oxygen ($O_x \equiv O_3 + NO_2$) sensor. In addition, the NO_2-B42F sensor was found to possess a significant NO sensitivity (130%) that exceeds the cross-sensitivity specified in the Alphasense documentation (<5%). The NO_2-B43F sensor was found to have 0.002% sensitivity to CO_2 gas, which is in the range of the cross-sensitivity specified in the Alphasense documentation (<0.1%). However, given
10   that typical ambient CO_2 concentrations are four orders of magnitude larger than NO_2 concentrations, this relatively small cross-sensitivity to CO_2 gas manifests as a significant interference in the NO_2 sensors. These cross-sensitivities are represented in Eqn. 3 and Eqn. 4.

Temperature Dependence – Electrochemical sensors are known to have temperature dependent sensitivities and zero offsets.
15   Alphasense reports sensitivities and zero offsets for a temperature range between -30 °C and 50 °C. The sensitivities in their data sheets vary with temperature by +0.1 to +0.3 %/K (referenced to sensitivity at 20 °C) and the zero offsets are indicated to vary little except at high temperatures. We observed similar, but slightly larger variations via in situ comparison to co-located reference instruments. We observed temperature dependence in the sensitivities of +0.3 to +5 %/K and no variation in the zero offset of the CO, NO_2, and O_3 sensors from 10 °C to 24 °C (Fig. 3). However, the zero offset of the NO sensor
20   exhibited a strong temperature dependence of 0.34 mV/K.

Drift – Two laboratory calibrations were performed roughly 10 weeks apart and the zero offsets and sensitivities are shown in Table 1. Over the 10-week interval, zero drift was equivalent to -15.9 ppb, -2.3 ppb, +15.8 ppb, and -12.7 ppb for CO, NO, NO_2, and O_3, respectively. Alphasense reports the stability over time for the zero offset to be < ±100, 0 to 50, 0 to 20,
25   and 0 to 20 ppb yr^{-1} for these sensors, respectively; over this 10 week interval, the observed zero drift was within the range of these specifications. However, it is a large fraction of the annual drift specification and further experiments would be warranted to test whether the zero measured is stable over a full year within the specified tolerances. The drift in the sensitivity (in % of k_X) was -15.9%, -17.7%, -20.6%, and -53.2%. Alphasense reports <10, 0 to -20, -20 to -40, and < -20 to -40% yr^{-1} for CO, NO, NO_2, and O_3 calibration factors, respectively. We find that drift for the CO and O_3 sensitivities
30   exceeded the manufacturer specifications, but that the NO and NO_2 sensitivity drifts were within the specified tolerances.

5

3 Model for Field Calibration

Here, we propose a model for field calibration that leverages (1) useful cross-sensitivities, (2) chemical conservation equations, (3) knowledge of the global and/or regional background of pollutants, and (4) assumptions based on well-known characteristics of urban air quality and local emissions. The result is a calibration procedure for the drift and temperature dependencies of the 10 calibration parameters that does not require co-location with a reference instrument or prior laboratory experiments for each sensor. The first constraint we apply is the O_3 sensors' cross-sensitivity to NO_2. Laboratory measurements indicate that this cross-sensitivity is 100% and we fix it at that value.

3.1 Regional ozone uniformity to calibrate the NO_2 and O_3 sensors' sensitivities

The NO, NO_2, and O_3 sensitivity can be derived from observations with higher quality instruments at nearby locations. Ozone is a secondary pollutant with small local scale variation, except in the very near field of NO emissions. The Bay Area Air Quality Management District (BAAQMD) maintains four TECO 49i ozone analyzers within the BEACO$_2$N study area (see Fig. 1). We choose the closest site among these four regulatory monitoring sites to provide $O3_{ambient}$ as a constraint for multiple linear regression of Eqn. 5 (derived from Eqn. 2-4). Different BEACO$_2$N nodes are thus referenced to different reference instruments.

$$O3_{ambient} = \frac{V_{O_3}}{k_{O_3}} - \frac{V_{NO_2}}{k_{NO_2}} + r_{NO-NO_2}\frac{V_{NO}}{k_{NO}} - offset \tag{5}$$

Here, $offset$ is a combination of the zero offsets of the NO, NO_2, and O_3 sensors, all of which can be constrained as detailed in Sect. 3.2 below. The sensitivity of the O_3 and NO_2 sensors (k_{O_3} and k_{NO_2}), and relationship between the NO-NO_2 cross-sensitivity and the sensitivity of the NO sensor (r_{NO-NO_2}/k_{NO}) are obtained by multiple linear regression of Eqn. 5.

3.2 Use of co-emitted gases in plumes to calibrate the CO and NO sensors' sensitivity

The CO and NO sensor cannot be constrained by cross sensitivity to the other gases. Instead, we constrain the sensitivity by insisting that the median emission factor of CO (or NO) per unit CO_2 corresponds to median values reported for the U.S. vehicle fleet. We express the emission factor ($EF_X, ppb\ ppm^{-1}$) of gas X, which is CO or NO, as in Eqn. 8:

$$EF_X = \frac{\Delta X_{ambient}}{\Delta CO2_{ambient}} = \frac{1}{k_X}\frac{\Delta V_X}{\Delta CO2_{ambient}} \tag{6}$$

Our measurements of the concentration of CO_2 are described in Shusterman et al. (2016) and values for EF_{CO} and EF_{NO_x} are reported in Dallmann et al. (2013; see Table 2). We constrain the sensitivity of the CO and NO sensors in the network such that the median $\Delta X/\Delta CO_2$ of the plumes are equal to emission factors characteristic of the average vehicle fleet. The NO sensors' sensitivity is constrained by the emission factor of NO_X, estimating the upper limit of NO concentration.

6

Figure 4 shows an example of a measured plume and the derived $\Delta CO/\Delta CO_2$ ratio. We identify plumes as the local maximum found in a 10-minute moving window, starting and ending at the local minima. Each plume is a few minutes in duration, representing an emission ratio averaged over several vehicles. Since diesel trucks have an order of magnitude higher NO_X emission factors compared to gasoline vehicles, the percentage of truck traffic near each site affects the median emission factors. The median freeway truck ratio varies little across the $BEACO_2N$ network, however, regions with a larger range of median truck ratios will have larger uncertainties or require a calibration approach that accounts for this variation.

3.3 Use of chemical conservation equations near emissions to calibrate the NO, NO_2 and O_3 sensors' zero offsets

We are able to constrain the zero offsets of NO, NO_2 and O_3 sensors by taking advantage of proximity to local emission sources and the following chemical conservation equations.

$$NO + O_3 \rightarrow NO_2 + O_2 \tag{R1}$$

$$NO_2 + hv \rightarrow NO + O \tag{R2}$$

$$O + O_2 + M \rightarrow O_3 + M \tag{R3}$$

These three reactions result in a steady-state relationship among the nitrogen oxides ($NO_X \equiv NO + NO_2$) and ozone. At nighttime, reaction R2 does not occur due to the absence of sunlight. In the absence of emissions, the NO concentration goes to zero on nights with sufficient O_3. Conversely, near strong emission sources, NO is found in excess of ozone and the O_3 concentration goes to zero (see Fig. 5). Using this logic, we identify times between 12 am to 3 am when there is zero NO or O_3 to define the zero offsets of the NO and O_3 sensors, using 1-minute averaged data with plumes excluded (see Sect. 3.3 for details of the plume identification procedure).

The NO_2 offset can be determined using the pseudo-steady state (PSS) approximation. We estimate the NO_2 concentration through Eqn. 7:

$$j_{NO_2}[NO_2] = k_{NO-O_3}[NO][O_3] \tag{7}$$

Here, j_{NO_2} (in units of s^{-1}) is the photolysis rate constant for reaction R2 and k_{NO-O_3} (in units of cm^3 molecule^{-1} s^{-1}) is the rate constant for reaction R1. $[X]$ expresses the concentration of gas X in units of molecules cm^{-3}. We use sensitivity corrected (see Section 3.1 and 3.2), 1-minute average NO and O_3 concentrations measured from 12 pm to 3 pm, and select data with a time derivative of O_3 near zero to insure that the measurements reflect air that has achieved steady state. The NO_2 concentration at PSS is derived using Eqn. 7 and the NO_2 offset is chosen to insure the calculated and observed NO_2 are equal. NO_2 is also produced through the reaction of HO_2/RO_2 with NO, but this is omitted from the right hand side of Eqn. 7, resulting in a lower bound of the true NO_2 concentration. Estimated NO_2 is therefore low by about 5% in winter and as much as 30% in summer. If higher accuracy is needed, the reaction of HO_2/RO_2 with NO could be considered to reduce this bias.

3.4 Use of global background to calibrate the CO sensors' zero offset

To infer the zero offset of the CO sensor, we follow the procedure outlined in Shusterman et al. (2016) for CO_2 sensors. We assume the signal measured at a given site is decomposed as in Eqn. 8:

$$[CO]_{ambient} = [CO]_{background} + [CO]_{local} + offset \tag{8}$$

The measurement of the pollutant CO ($[CO]_{ambient}$) is the sum of regional and local signals ($[CO]_{background}$ and $[CO]_{local}$, respectively), as well as some offset from the true concentration ($offset$). Assuming the monthly minimum concentration measured at a given site represents $[CO]_{background}$, this background signal is compared to that measured at a "supersite" of reference instruments located within the network domain, allowing the offset to be derived. We also assume that when $[CO]_{ambient}$, as well as $[CO]_{local}$, is minimum in each day, the concentration measured at a given site has a constant deviation from the background signal. This is a reasonable assumption for the BEACO₂N domain as the dominant wind pattern frequently brings unpolluted air from the Pacific Ocean.

3.5 Temperature dependence and temporal drift

In order to account for the temperature and time dependence of calibration parameters, we apply the calibration process described in Sect. 3.1 through 3.4 for temperature increments of 1°C within a 3-month running window. Then, we are able to define a temperature dependent sensitivity and zero offset, which is used to convert the measured voltages to mixing ratios. In this way, we can also evaluate temporal drift with monthly resolution. The calibration procedure can be repeated for shorter time intervals if wider temperature windows are used.

4 Evaluation with reference observations

We evaluate the efficacy of our calibration method using a BEACO₂N node co-located with reference instruments at the Laney College monitoring site maintained by the Bay Area Air Quality Management District (BAAQMD). Here we consider data collected from February to April 2016, calibrate it according to the procedure described above (following Sect. 3.1 to 3.5), and compare it against the BAAQMD data. Reference data is collected by a TECO 48i CO analyzer and a TECO 42i NO$_x$ analyzer. Ozone data from the "Oakland West" location, the closest ozone-monitoring site maintained by BAAQMD, was used for multiple linear regression of Eqn. 5. The zero offset for CO was calculated using BAAQMD data from the Bodega Bay background site (see Fig. 1; Guha et al., 2016) as local "supersite" data was unavailable during this period. A background site closer to the network would likely improve our ability to constrain the CO zero offset; a reference instrument for that purpose was installed in summer 2017.

In our calibration procedure, the cross-sensitivities and temperature dependence are corrected for better accuracy. Table 3 shows the reduction in mean absolute error (MAE) that results when cross-sensitivity and temperature dependence issues are

8

considered during multiple linear regression of Eqn. 5. Here, MAE is calculated after conducting the sensitivity correction explained in Section 3.1, but before the offset correction in Section 3.3. Fully calibrated, hourly averaged BEACO$_2$N sensor data is compared to reference data in Fig. 6. For NO, NO$_2$, O$_3$, and CO the mixing ratio measured agrees reasonably well with the reference instrument with correlation coefficients of 0.88, 0.61, 0.69, and 0.74 and MAE of 3.63 ppb, 4.12 ppb, 5.04

5   ppb, and 54.93 ppb, respectively. The noise ($\pm 2\sigma$) in the differences between the calibrated hourly BEACO$_2$N data and reference data is 9.74 ppb for NO, 9.97 ppb for NO$_2$, 13.04 ppb for O$_3$, and 116.23 ppb for CO. These noise values are dominated by the Alphasense noise except in the case of CO, where noise is evenly split between the low-cost electrochemical sensors and the reference instruments.

5 Examples of network performance

10   Figure 7 shows a week-long time series of fully calibrated air quality data from four BEACO$_2$N sites in 2017 (see Fig. 1). BEACO$_2$N nodes capture the short-term variability associated with local emissions, superimposed on the diurnal variation caused by mixing and changes in the height of the boundary layer. Large mixing ratios of NO, NO$_2$, and O$_3$ are observed at the Hercules and Ohlone sites, likely representing strong NO$_x$ emissions from an oil refinery nearby. The spatial variability of trace gases observed at these 4 BEACO$_2$N sites provides a more diverse perspective on emissions compared to that

15   provided by the one regulatory monitoring site in the vicinity.

The emission ratios of CO and NO$_x$ were also investigated using the BEACO$_2$N data from sample locations. Figure 8 shows ratios observed at the Laney College site. The slope of CO/NO$_x$ varies from 4.43 to 12.99 across 5 BEACO$_2$N sites, reflecting spatial variations in local sources. Sites near roads with more diesel vehicles, such as Laney College, show lower

20   CO/NO$_x$ ratios, as expected given diesel vehicles' higher NO$_x$ emissions. The range of observed CO/NO$_x$ emission ratios is similar to the values reported by McDonald et al. (2013).

6 Conclusion

Calibration of low-cost sensors is necessary for quantitative analysis. In this paper, we have described a truly low cost, routine in-field calibration method and the evaluation of a fully calibrated low-cost, high-density air quality sensor network.

25   The Alphasense B4 electrochemical gas sensors are able to detect typical diurnal cycles in gas concentrations as well as short-term changes corresponding to chemical reactions and local emissions. These capabilities of the sensors are utilized for a field calibration protocol that does not require co-location with reference instrumentation, but does require reference instruments to be sited within the network domain. The calibrated dataset demonstrates the accuracy required to resolve information relevant to urban emission sources, such as CO/NO$_x$ emission ratios. Through this work, we can realize the

30   promise of low-cost, high-density sensor networks as a viable approach for atmospheric monitoring.

Acknowledgements

References

Bart, M., Williams, D. E., Ainslie, B., Mckendry, I., Salmond, J., Grange, S. K., … Henshaw, G. S. (2014). High Density Ozone Monitoring Using Gas Sensitive Semi-Conductor Sensors in the Lower Fraser Valley, British Columbia.
10   *Environmental Science and Technology*, *48*, 3970–3977.

Borrego, C., Costa, A. M., Ginja, J., Amorim, M., Coutinho, M., Karatzas, K., … Elen, B. (2016). Assessment of air quality microsensors versus reference methods : The EuNetAir joint exercise. *Atmospheric Environment*, *147*(2), 246–263. http://doi.org/10.1016/j.atmosenv.2016.09.050

Cox, R. M. (2003). The use of passive sampling to monitor forest exposure to O 3 , NO 2 and SO 2 : a review and some case
15   studies . *Environmental Pollution*, *126*(2), 301–311. http://doi.org/10.1016/S0269-7491(03)00243-4

Cross, E. S., Lewis, D. K., Williams, L. R., Magoon, G. R., Kaminsky, M. L., Worsnop, D. R., & Jayne, J. T. (2017). Use of electrochemical sensors for measurement of air pollution : correcting interference response and validating measurements. *Atmospheric Measurement Techniques Discussions*, (May), 1–17. http://doi.org/10.5194/amt-2017-138

Dallmann, T. R., Demartini, S. J., Kirchstetter, T. W., Herndon, S. C., Onasch, T. B., Wood, E. C., & Harley, R. A. (2012).
20   On-Road Measurement of Gas and Particle Phase Pollutant Emission Factors for Individual Heavy-Duty Diesel Trucks. *Environmental Science and Technology*, *46*, 8511–8518.

Dallmann, T. R., Harley, R. A., & Kirchstetter, T. W. (2011). Effects of Diesel Particle Filter Retrofits and Accelerated Fleet Turnover on Drayage Truck Emissions at the Port of Oakland. *Environmental Science and Technology*, 10773–10779.

Dallmann, T. R., Kirchstetter, T. W., Demartini, S. J., & Harley, R. A. (2013). Quantifying On-Road Emissions from
25   Gasoline-Powered Motor Vehicles: Accounting for the Presence of Medium- and Heavy-Duty Diesel Trucks. *Environmental Science and Technology*, *47*, 13873–13881.

Hagan, D. H., Issacman-vanwertz, G., Franklin, J. P., Wallace, L. M. M., Kocar, B. D., Heald, C. L., & Kroll, J. H. (2017). Calibration and assessment of electrochemical air quality sensors by co-location with reference-grade instruments. *Atmospheric Measurement Techniques Discussions*, *2*(August), 1–40.

30   Holstius, D. M., Pillarisetti, A., Smith, K. R., & Seto, E. (2014). Field calibrations of a low-cost aerosol sensor at a regulatory monitoring site in California. *Atmospheric Measurement Techniques*, *7*, 1121–1131. http://doi.org/10.5194/amt-7-1121-2014

Jerrett, M., Donaire-gonzalez, D., Popoola, O., Jones, R., Cohen, R. C., Almanza, E., … Nieuwenhuijsen, M. (2017). Validating novel air pollution sensors to improve exposure estimates for epidemiological analyses and citizen science. *Environmental Research*, *158*(April), 286–294. http://doi.org/10.1016/j.envres.2017.04.023

Jiao, W., Hagler, G., Williams, R., Sharpe, R., & Brown, R. (2016). Community Air Sensor Network (CAIRSENSE) project : Evaluation of low-cost sensor performance in a suburban environment in the southeastern United States. *Atmospheric Measurement Techniques*, *9*, 5281–5292. http://doi.org/10.5194/amt-9-5281-2016

Krupa, S. V, & Legge, A. H. (2000). Passive sampling of ambient , gaseous air pollutants : an assessment from an ecological perspective. *Environmental Pollution*, *107*, 31–45.

Lateb, M., Meroney, R. N., Yataghene, M., Fellouah, H., Saleh, F., & Boufadel, M. C. (2016). On the use of numerical modelling for near-field pollutant dispersion in urban environments. A review. *Environmental Pollution*, *208*, 271–283. http://doi.org/10.1016/j.envpol.2015.07.039

Masson, N., Piedrahita, R., & Hannigan, M. (2015). Chemical Approach for quantification of metal oxide type semiconductor gas sensors used for ambient air quality monitoring. *Sensors & Actuators B: Chemical*, *208*, 339–345. http://doi.org/10.1016/j.snb.2014.11.032

Mcdonald, B. C., Gentner, D. R., Goldstein, A. H., & Harley, R. A. (2013). Long-Term Trends in Motor Vehicle Emissions in U.S. Urban Areas. *Environmental Science and Technology*, *47*(17), 10022–31. http://doi.org/10.1021/es401034z

Mead, M. I., Popoola, O. A. M., Stewart, G. B., Landshoff, P., Calleja, M., Hayes, M., … Jones, R. L. (2013). The use of electrochemical sensors for monitoring urban air quality in low-cost , high-density networks. *Atmospheric Environment*, *70*, 186–203. http://doi.org/10.1016/j.atmosenv.2012.11.060

Michael, M., Jonas, M., & Christoph, H. (2017). Design of an ozone and nitrogen dioxide sensor unit and its long-term operation within a sensor network in the city of Zurich. *Atmospheric Measurement Techniques Discussions*, (March). http://doi.org/10.5194/amt-2017-22

Mijling, B., Jiang, Q., Jonge, D. De, & Bocconi, S. (2017). Practical field calibration of electrochemical NO 2 sensors for urban air quality applications. *Atmospheric Measurement Techniques Discussions*, (2). http://doi.org/10.5194/amt-2017-43

Moltchanov, S., Levy, I., Etzion, Y., Lerner, U., Broday, D. M., & Fishbain, B. (2015). On the feasibility of measuring urban air pollution by wireless distributed sensor networks. *Science of the Total Environment, The*, *502*, 537–547. http://doi.org/10.1016/j.scitotenv.2014.09.059

Papapostolou, V., Zhang, H., Feenstra, B. J., & Polidori, A. (2017). Development of an environmental chamber for evaluating the performance of low-cost air quality sensors under controlled conditions. *Atmospheric Environment*, *171*, 82–90. http://doi.org/10.1016/j.atmosenv.2017.10.003

Piedrahita, R., Xiang, Y., Masson, N., Ortega, J., Collier, A., Jiang, Y., … Hannigan, M. (2014). The next generation of low-cost personal air quality sensors for quantitative exposure monitoring. *Atmospheric Measurement Techniques*, *3*(2), 3325–3336. http://doi.org/10.5194/amt-7-3325-2014

Sadighi, K., Coffey, E., Polidori, A., Feenstra, B., Lv, Q., & Henze, D. K. (2017). Intra-urban spatial variability of surface ozone and carbon dioxide in Riverside , CA : viability and validation of low-cost sensors. *Atmospheric Measurement Techniques Discussions*, (August), 1–30.

Shusterman, A. A., Teige, V. E., Turner, A. J., Newman, C., Kim, J., & Cohen, R. C. (2016). The BErkeley Atmospheric CO 2 Observation Network : initial evaluation. *Atmospheric Chemistry and Physics*, 13449–13463. http://doi.org/10.5194/acp-16-13449-2016

Spinelle, L., Gerboles, M., Gabriella, M., & Aleixandre, M. (2015). Field calibration of a cluster of low-cost available sensors for air quality monitoring. Part A : Ozone and nitrogen dioxide. *Sensors & Actuators B: Chemical*, *215*, 249–257. http://doi.org/10.1016/j.snb.2015.03.031

Spinelle, L., Gerboles, M., Gabriella, M., & Aleixandre, M. (2017). Field calibration of a cluster of low-cost commercially available sensors for air quality monitoring . Part B : NO, CO and CO 2. *Sensors & Actuators B: Chemical*, *238*(2), 706–715. http://doi.org/10.1016/j.snb.2016.07.036

Sun, L., Wong, K. C., Wei, P., Ye, S., Huang, H., & Yang, F. (2015). Development and Application of a Next Generation Air Sensor Network for the Hong Kong Marathon 2015 Air Quality Monitoring. *Sensors*, *16*(211). http://doi.org/10.3390/s16020211

Vardoulakis, S., Fisher, B. E. A., Pericleous, K., & Gonzalez-flesca, N. (2003). Modelling air quality in street canyons : a review. *Atmospheric Environment*, *37*, 155–182.

Wild, R. J., Dub, W. P., Neuman, J. A., Peischl, J., Ryerson, T. B., & Brown, S. S. (2017). On-road measurements of vehicle NO 2 / NO x emission ratios in Denver, Colorado, USA. *Atmospheric Environment*, *148*(2), 182–189. http://doi.org/10.1016/j.atmosenv.2016.10.039

Williams, D. E., Henshaw, G. S., Bart, M., Laing, G., Wagner, J., Naisbitt, S., & Salmond, J. A. (2013). Validation of low-cost ozone measurement instruments suitable for use in an air-quality monitoring network. *Measurement Science and Technology*, *24*. http://doi.org/10.1088/0957-0233/24/6/065803

Zimmerman, N., Presto, A. A., Kumar, S. P. N., Gu, J., Hauryliuk, A., Ellis, S., … Subramanian, R. (2017). Closing the gap on lower cost air quality monitoring : machine learning calibration models to improve low-cost sensor performance. *Atmospheric Measurement Techniques Discussions*, (2), 1–36.
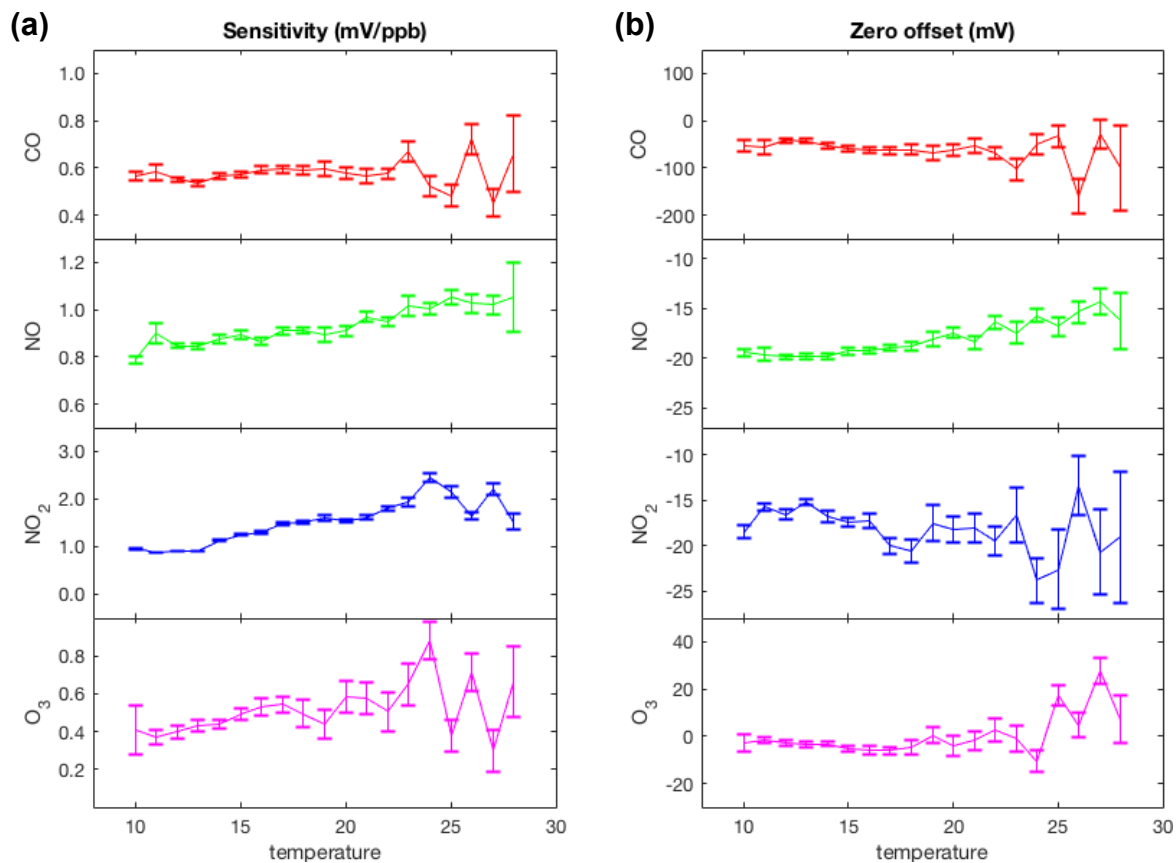
12
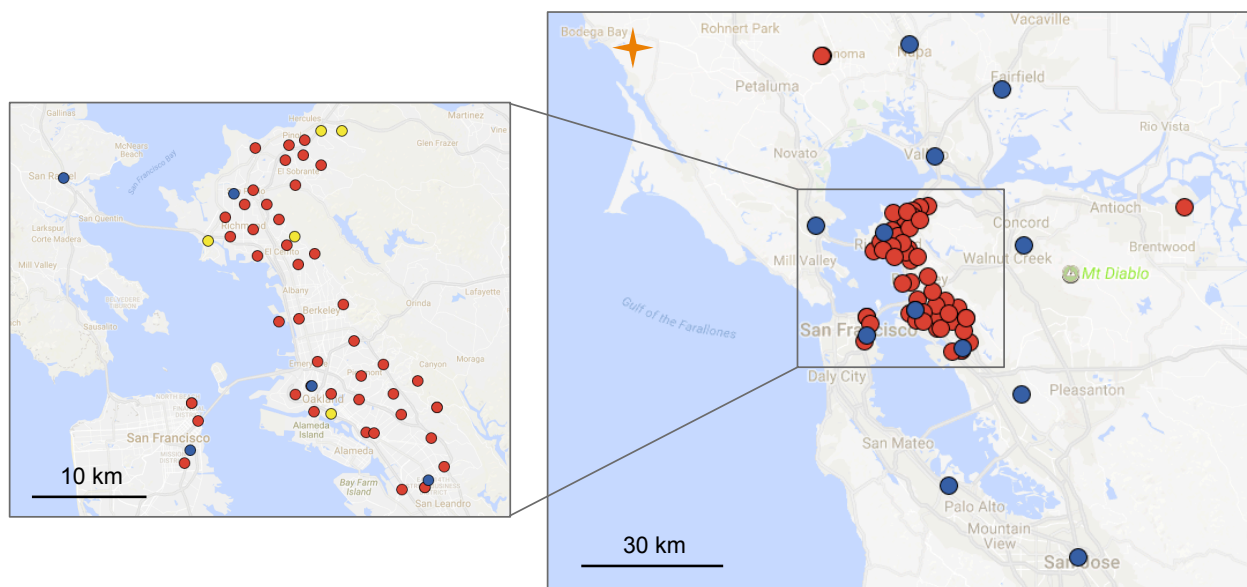
Figure 1: Map of San Francisco Bay Area showing current BEACO$_2$N node sites (red), BAAQMD reference sites with O$_3$ measurements (blue), and the BAAQMD Bodega Bay regional greenhouse gas background site (orange). The sites used in this analysis are marked in yellow on the detailed panel.

5
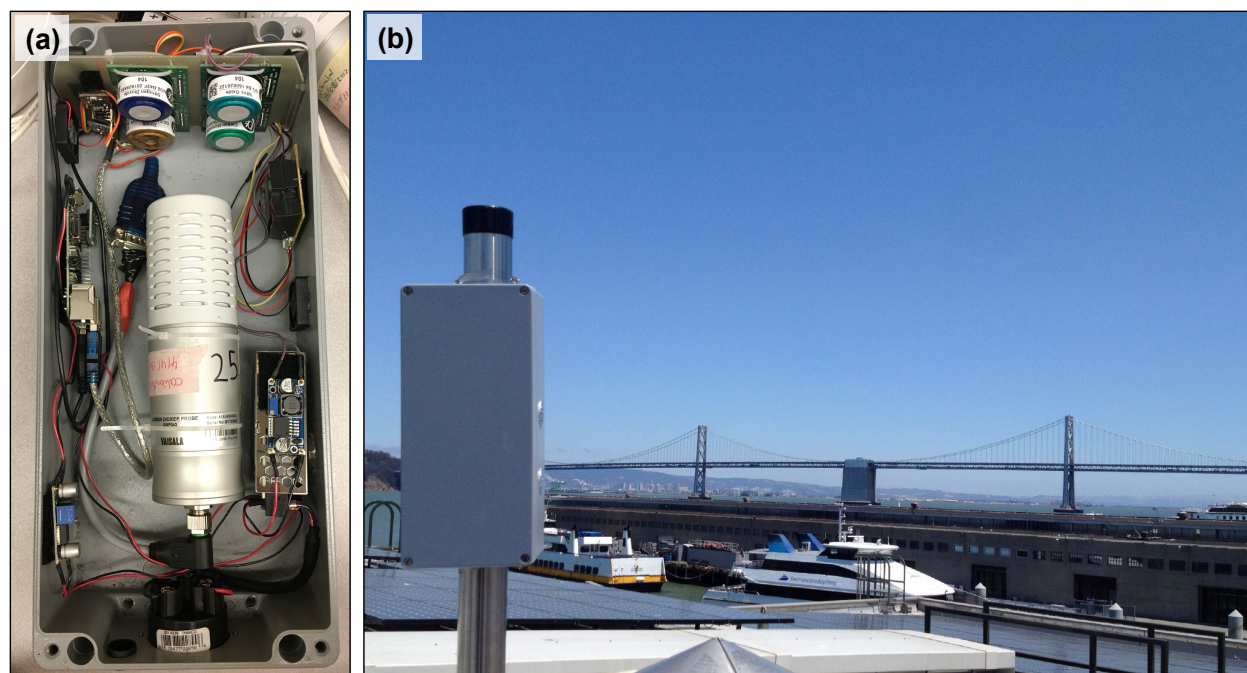
Figure 2. (a) Current BEACO$_2$N node design and (b) a photo of a node deployed.

Figure 3. Representative temperature dependent sensitivities (a) and zero offsets (b) of the Alphasense electrochemical sensors calculated by comparing hourly averaged measurements from Laney College BEACO₂N node to measurements from a co-located reference instrument during February to April 2016.

5
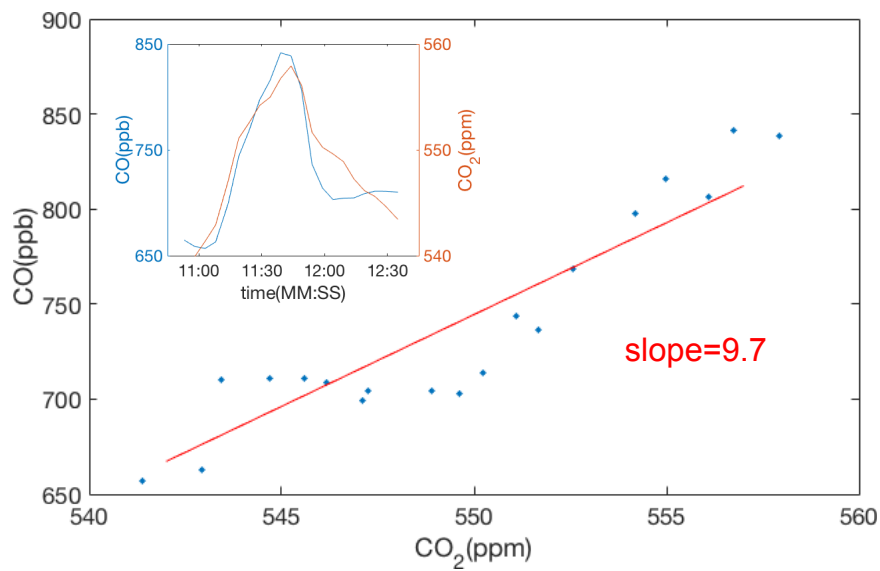
Figure 4. Example of CO plume identification and regression against CO_2 to find the CO emission factor using raw, 10-second data. The derived CO emission ratio (CO/CO_2) for this example is 9.7 ppb ppm^{-1}.
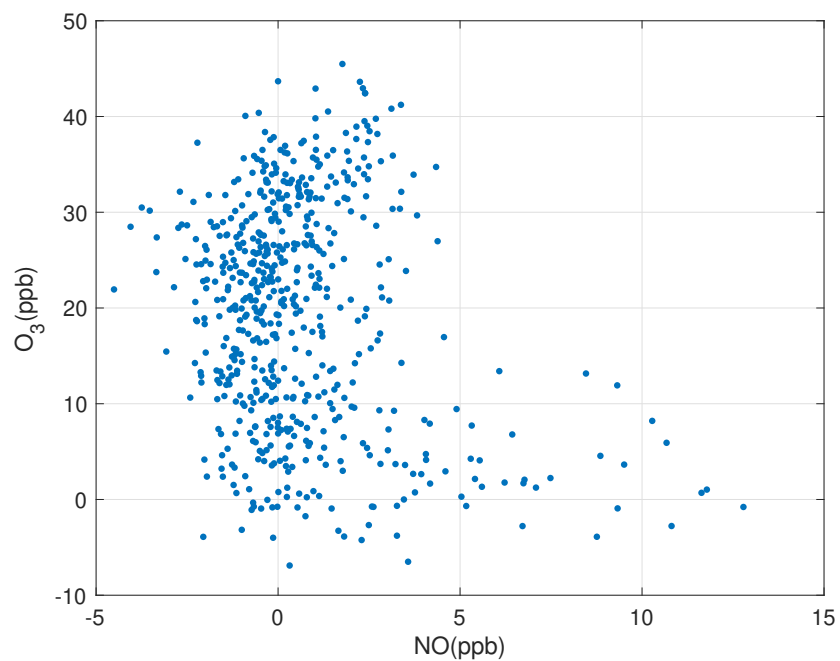
Figure 5. Representative month of 1-minute averaged NO and O_3 measurements taken between 12 and 3 am; plumes excluded.

15
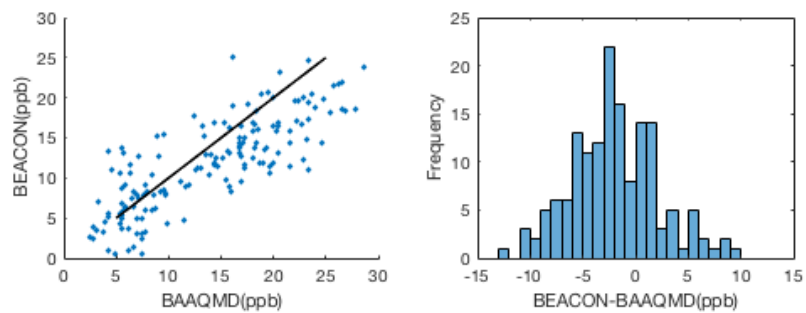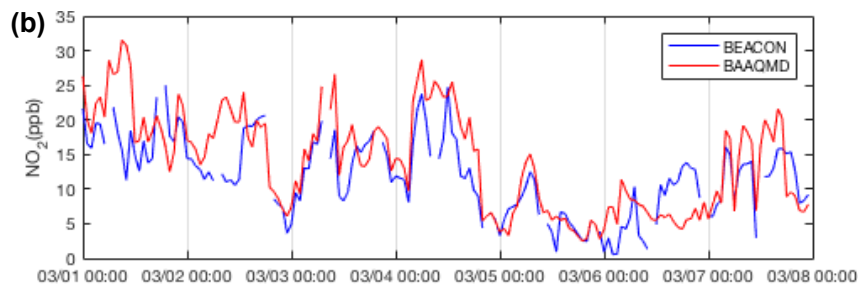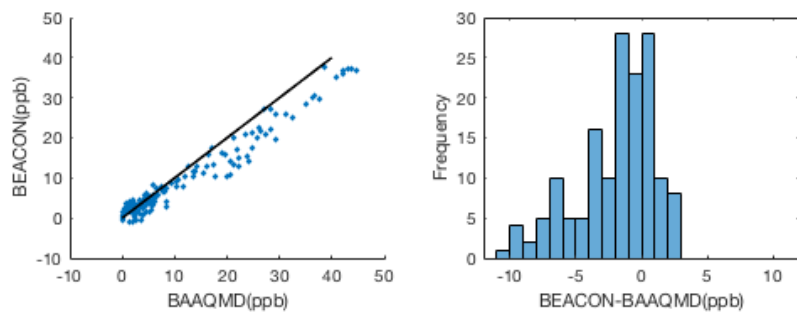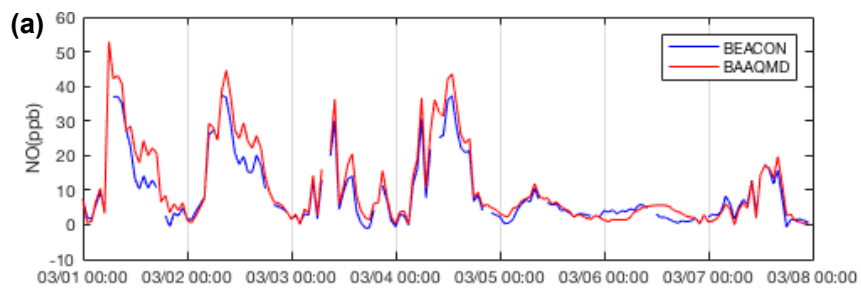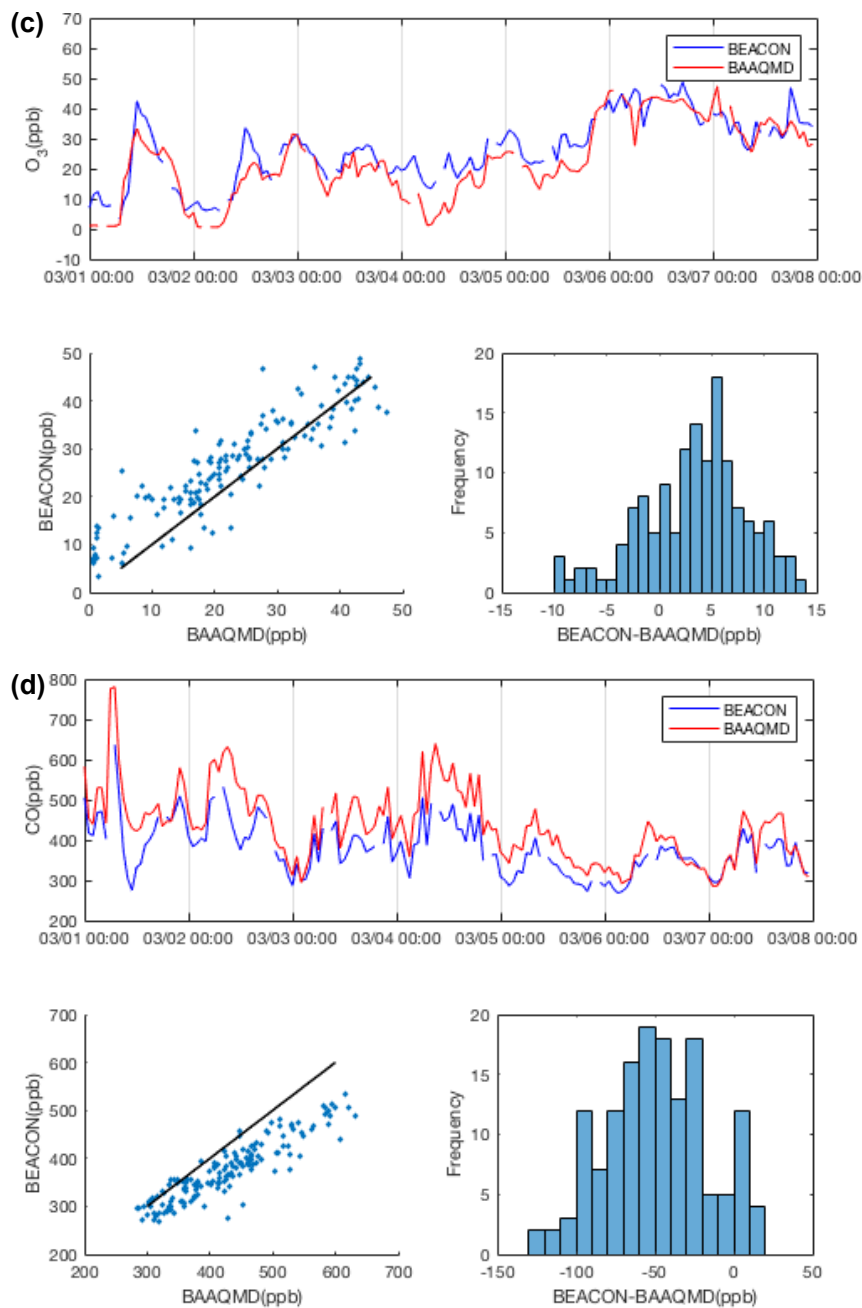
Figure 6. Time series (top), direct comparison (bottom left), and histogram (bottom right) of hourly averaged (a) NO, (b) NO₂, (c) O₃, (d) CO mixing ratios from a representative week of calibrated BEACO₂N and BAAQMD reference data. Black line in bottom left plot indicates the 1:1 line.
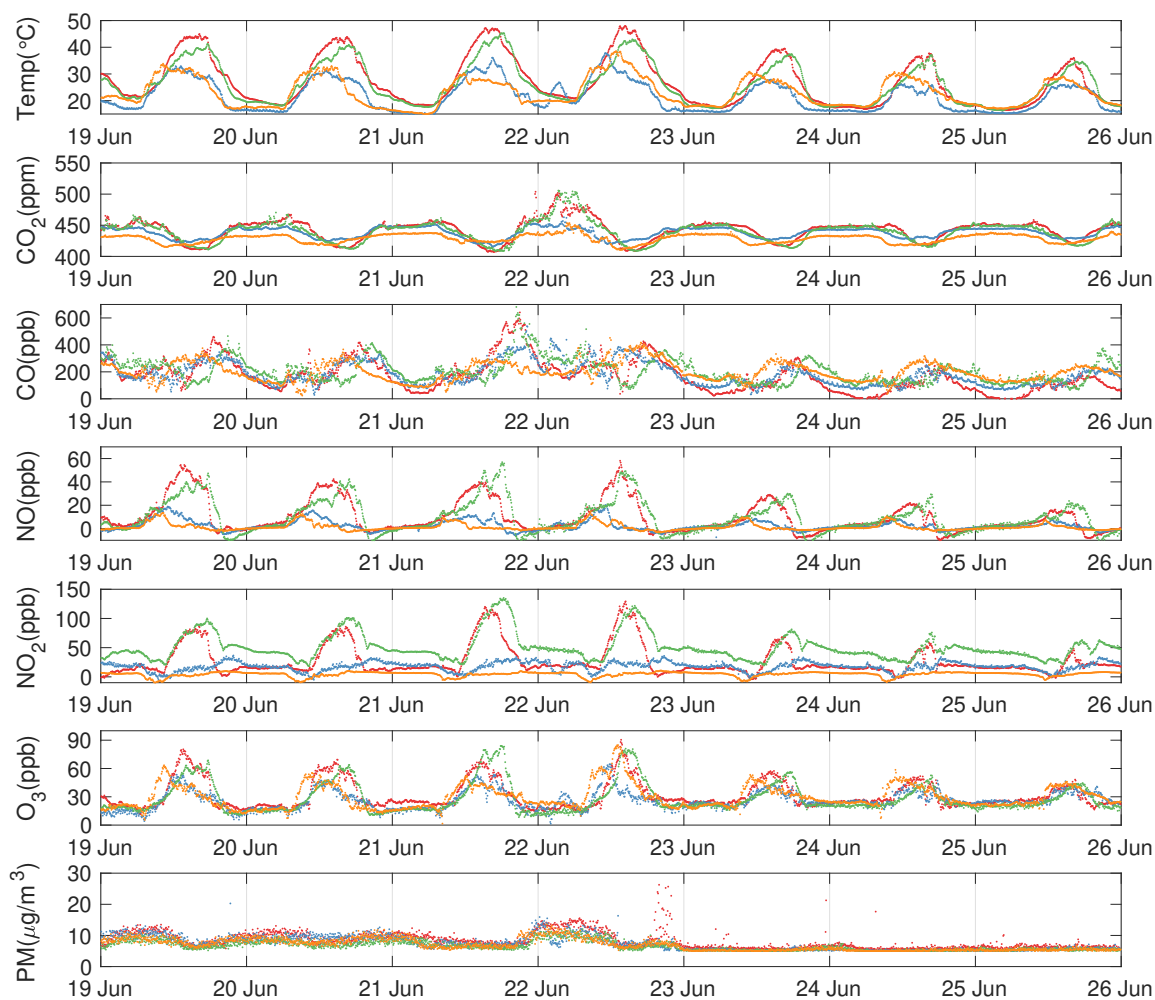
Figure 7. Time series of fully calibrated 5-minute averaged BEACO$_2$N data from a representative week at 4 sites deployed in 2017. Observations from the Hercules, Ohlone, Washington, and Madera sites are plotted in red, green, orange, and blue, respectively. Particulate matter is converted to units of mass concentration according to Holstius et al (2014).

5

18
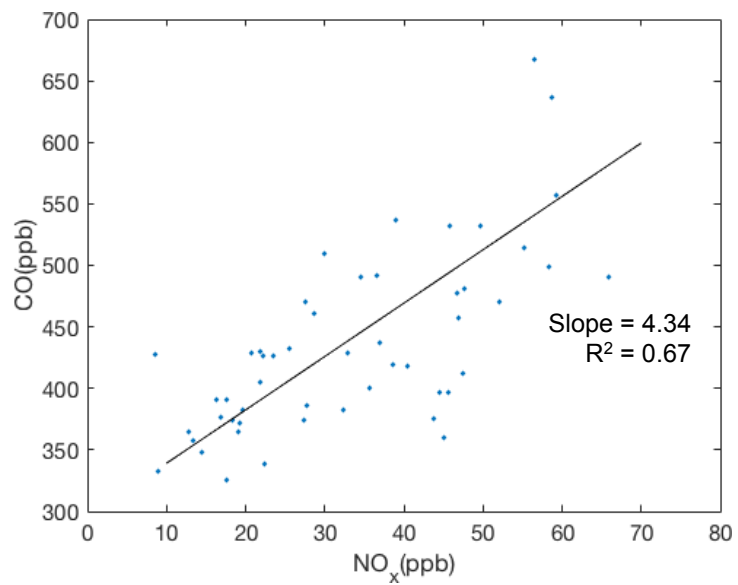
Figure 8. CO vs. NO$_x$ measured at Laney College between 8 am and 10 am.

Table 1. Zero offsets and sensitivities of a representative quartet of Alphasense B4 electrochemical sensors derived via comparison to delivered reference gases during two separate laboratory calibration separated by an approximately 10-week interlude.

		May	August
O_3	Zero offset (mV)	-34.6417	-42.7629
	Sensitivity (mV/ppb)	0.6404	0.2997
CO	Zero offset (mV)	108.9770	89.5812
	Sensitivity (mV/ppb)	1.2192	1.0301
NO	Zero offset (mV)	-14.2030	-17.7801
	Sensitivity (mV/ppb)	1.5758	1.2972
NO_2	Zero offset (mV)	-13.7159	-6.0649
	Sensitivity (mV/ppb)	0.4842	0.3843

Table 2. Reported emission factors of diesel and gasoline vehicles (Dallmann et al., 2011; Dallmann et al., 2012; Dallmann et al., 2013). Emissions from medium-duty and heavy-duty diesel trucks, which account for <1% of all vehicles, were removed to give the value for light-duty gasoline vehicles.

Vehicle Type	CO emission factor ($g\ kg^{-1}_{fuel}$)	NO_X emission factor ($g\ kg^{-1}_{fuel}$)
Heavy-duty Diesel Trucks	8.0 ± 1.2	28.0 ± 1.5
Light-duty Gasoline Vehicles	14.3 ± 0.7	1.90 ± 0.08
99% Gasoline Vehicles, 1% Diesel Trucks	14.2 ± 0.7	2.29 ± 0.12

Table 3. Mean absolute error of comparison between regional O_3 and hourly averaged BEACO$_2$N O_3 measurements derived from multiple linear regression models of increasing complexity between February and April 2016.

Regression Models		Mean absolute error (ppb)
$O3_{true} = \dfrac{V_{O3}}{k_{O3}} - offset$	Linearity of observed voltages and gas concentration	14.4063
$O3_{true} = \dfrac{V_{O3}}{k_{O3}} - \dfrac{V_{NO2}}{k_{NO2}} - offset$	O_3 sensor's cross-sensitivity correction	10.6795
$O3_{true} = \dfrac{V_{O3}}{k_{O3}} - \dfrac{V_{NO2}}{k_{NO2}} + r_{NO-NO2}\dfrac{V_{NO}}{k_{NO}} - offset$	NO_2 and O_3 sensor's cross-sensitivity correction	8.8172
$O3_{true} = \dfrac{V_{O3}}{k_{O3}} - \dfrac{V_{NO2}}{k_{NO2}} + r_{NO-NO2}\dfrac{V_{NO}}{k_{NO}} - offset$	Adding temperature correction	8.1360